# Catalyst Preparation Procedure Probed by EXAFS Spectroscopy. 2. Cobalt on Titania

**Kazuyuki Tohji,[1a] Yasuo Udagawa,*[1a] Shuji Tanabe,[1b] Takashi Ida,[1b] and Akifumi Ueno[1b]**

*Contribution from the Institute for Molecular Science, Myodaiji, Okazaki, Aichi 444, Japan, and Toyohashi University of Technology, Toyohashi, Aichi 440, Japan.* *Received January 3, 1984*

**Abstract:** Extended X-ray absorption fine structure (EXAFS) was used, in combination with electron microscopy, NMR, and X-ray diffraction, to probe environments of Co atoms at every elementary step of the preparation procedure for $TiO_2$ supported Co catalyst. Special emphasis was placed on the relationship between the particle size and the methods, and conditions, of the catalyst preparation. The species which are formed during the course of the preparation were clearly identified, and it was found that a cluster size as small as about 8 Å can be estimated from the analysis of EXAFS spectra. It was also found that bulklike $Co_3O_4$, very tiny $Co_3O_4$ clusters, and complex oxide $CoTiO_3$ are formed by the calcination, depending on the preparation method and temperature. It is concluded that the precedent species of oxide and their sizes before reduction have strong effects on the size of metal particles in the resultant catalyst.

Catalysts consisting of small metal particles on the surface of carriers are widely used in industrial processes. Amorphous $Al_2O_3$ and $SiO_2$ have high specific surface areas and are most frequently used as a support material. $TiO_2$ also has a fairly large surface area and may serve as a carrier or a support with unique properties because of its known strong metal–support interaction.[2] Activity as well as selectivity are required for a catalyst of practical use, and it is well-known that the characteristics of a metal-supported catalyst strongly depend on the sizes of metal particles.[3] Hence, the development of techniques to control the metal particle size has been desired. The conventional method of preparation, the impregnation method, usually gives a catalyst whose metal particle size distribution is quite broad. One of the present authors found that the preparation procedure starting from metal alkoxide, which is called the alkoxide method, can supply supported metal catalysts with homogeneous metal size, and the size can be controlled by the metal concentration in the starting materials.[4]

In order to further develop the catalyst preparation technique, it is necessary to obtain an understanding of the structural reasons why the alkoxide method has an ability to control the metal particle size on the support. EXAFS is best suited for the purpose, because it can pursue local structure changes around a selected atomic species at every step of the preparation procedure, regardless of the phase of the intermediate products.

In the previous report[5] the structure changes during a $Ni/SiO_2$ preparation procedure were studied by using EXAFS spectroscopy for both the alkoxide and the impregnation method. It was found that the metal particle size of $Ni/SiO_2$ catalyst strongly depends upon the size and homogeneity of NiO clusters formed by the calcination process. The alkoxide method, which starts from a chain of chemical reactions in solution, makes it possible to distribute Ni atoms uniformly among the material, resulting in uniform distribution of small NiO clusters in the carrier when calcined. On the other hand, the impregnation method yields a fairly large NiO crystal by the calcination.

In this report $Co/TiO_2$ catalyst preparation procedures are studied in order to confirm whether the above conclusion is general or not. A more improved in-laboratory EXAFS facility than the one used previously was employed. It was observed that very fine $Co_3O_4$ clusters are formed in this case also at low calcination temperature in the alkoxide method. The oxide clusters are so small that the majority of the metal atoms exist near the surface, making the EXAFS spectrum clearly different from that of bulk oxide. In addition, it was observed that complex oxide $CoTiO_3$ is formed instead of $Co_3O_4$ at higher calcination temperature in this system. The two kinds of oxides show different behavior by the reduction; that is, the metal particle size grows with increasing temperature in the material containing tiny $Co_3O_4$ clusters, while the growth does not occur when $CoTiO_3$ is formed. This can be interpreted as an indication that the metal–support interaction increases with the calcination temperature.

On the other hand, bulklike $Co_3O_4$ and $CoTiO_3$ are formed depending on the calcination temperature in the impregnation method, and the metal size distribution of the reduced catalyst is broad. It is concluded that the species of these oxides and their sizes determine the structure of the catalyst which is prepared by the reduction of the oxide.

**Table I.** Preparation Procedures of $Co/TiO_2$ Catalyst by the Alkoxide and Impregnation Methods

| alkoxide method | impregnation method |
|---|---|
| a-1: $Co(NO_3)_2$ dissolved in ethylene glycol; kept stirred at 353 K for 4 h | i-1: impregnation of titania with $Co(NO_3)_2$ aqueous solution, followed by drying at 383 K overnight |
| a-2: addition of $(i\text{-}C_3H_7O)_4Ti$; kept stirred at 353 for 4 h; after the hydrolysis at 383 K for 4 h, a gel is formed | i-2: calcination in air at 723–973 K for 24 h |
| a-3: drying at 383 K for 24 h | i-3: reduction by $H_2$ at 723–973 K for 4 h |
| a-4: calcination in air at 723–973 K for 4 h | |
| a-5: reduction by $H_2$ at 723–973 K for 4 h | |

## Experimental Section and Data Analysis

Details of the preparation procedure of $Co/TiO_2$ catalyst through the alkoxide method have already been reported;[6] they are summarized in Table I as well as those of the impregnation method. Co concentrations of the catalysts prepared by both the methods are estimated to be about 10 wt % by X-ray fluorescence. The specific surface areas of the catalysts were determined by the BET method using $N_2$ at 77 K as 23.8 and 17.6 $m^2/g$ for the one prepared by the alkoxide method and the impregnation method, respectively.

The EXAFS spectrometer employed in this work is described elsewhere.[7] Basically it consists of a rotating anode X-ray generator (Rigaku

(1) (a) Institute for Molecular Science. (b) Toyohashi University of Technology.
(2) Tauster, S. J.; Fung, S. C.; Garten, R. J. *J. Am. Chem. Soc.* **1978**, *100*, 170–175.
(3) Delmon, B., Jacobs, P. A., Poncelet, G., Eds. "Preparation of Catalyst I, II"; Elsevier: Amsterdam, 1975, 1978.
(4) Ueno, A.; Suzuki, H.; Kotera, Y. *J. Chem. Soc., Faraday Trans. 1* **1983**, 127–138.
(5) Tohji, K.; Udagawa, Y.; Tanabe, S.; Ueno, A. *J. Am. Chem. Soc.* **1984**, *106*, 612–617.
(6) Takasaki, S.; Tanabe, S.; Takahashi, K.; Suzuki, H.; Ueno, A.; Kotera, Y. *J. Chem. Soc., Faraday Trans. 1*, in press.
(7) Tohji, K.; Udagawa, Y.; Kawasaki, T.; Masuda, K. *Rev. Sci. Instrum.* **1983**, *54*, 1482–1487.

0002-7863/84/1506-5172$01.50/0 

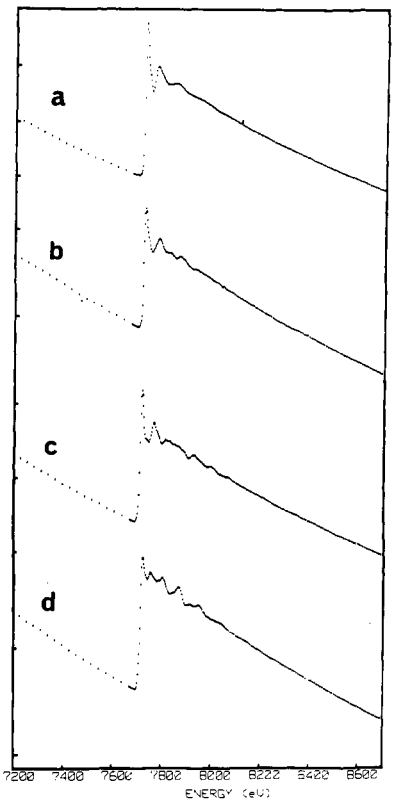


**Figure 1.** EXAFS spectra of the materials prepared during the course of $Co/TiO_2$ catalyst preparation by the alkoxide method: (a) dried sample at step a-3 of Table I, (b) calcined sample at 723 K at step a-4, (c) calcined sample at 973 K at step a-4, (d) reduced sample at step a-5.

RU-200), a spectrometer with a Johansson cut bent LiF(220) crystal, an ion chamber, slits, a pure Ge solid-state detector, and counting electronics, many of which are controlled by a microcomputer (SORD M223) through CAMAC bus. Absorbance $\mu x$ is obtained by the incident beam intensity $I_0$ and the transmitted photon number $I$ by $\mu x = \ln (I_0/I)$, where $x$ is the sample thickness. A partially transmitting ion chamber is used to detect $I_0$. The current from the ion chamber is detected by an electrometer (Keithley 616C) and changed to frequency by a V/F converter, and then the frequency is counted by a scaler. The photons which are transmitted by the sample are detected by an SSD (Ortec GLP-25440-s), and the signal is amplified by a fast amplifier (Ortec 460). After passing through a single channel analyzer (Ortec 553), the signal is counted by another scaler.

The X-ray source with an Ag target was operated at 17 kV and 150 mA in order to minimize the effect of higher order reflections on the ion chamber. With the receiving slit width of 200 $\mu$m, the resolution of the spectrometer is about 5 eV fwhm. Under these conditions the regular data acquisition time was about 2 h, collecting over $10^6$ counts ($I$) at each data point. Sometimes over $10^7$ counts were accumulated by an overnight measurement, reducing the statistical error to much less than 0.1%.

The liquid sample and the gel were kept between Mylar windows by the use of a copper spacer. The solid samples were prepared by pressing the powders into thin wafers by an IR pellet press. Boron nitride was used to dilute the sample if necessary.

In the analysis of the EXAFS spectra, the oscillatory part was subtracted, then converted to $k$ space, and Fourier transformed by the standard method, as described earlier.[5] The least-squares curve fitting with the back-transformed oscillation in $k$ space was performed by assuming the following formula derived from single-scattering theories[8,9]

$$\chi(k) = \sum_j \frac{N_j}{kr_j^2} \exp\left(-2\left(\sigma_j^2 k^2 + \frac{r_j}{\lambda}\right)\right) F_j(k) \sin(2kr_j + \phi_j(k)) \quad (1)$$

where $N_j$ is the number of atoms in the $j$th shell at distance $r_j$ from the central absorbing atom and $\sigma_j$ is the mean square deviation of the interatomic distance $r_j$. $F_j(k)$ and $\phi_j(k)$ are the backscattering amplitude and the phase shift, and the parameters obtained by the theoretical

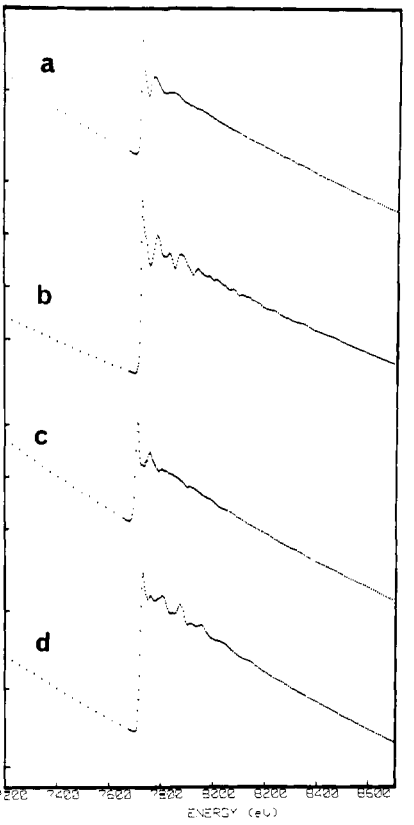


**Figure 2.** EXAFS spectra of the materials prepared during the course of the catalyst preparation by the impregnation method: (a) dried sample at step i-1 of Table I, (b) Calcined sample at 723 K at step i-2, (c) calcined sample at 973 K at step i-2, (d) reduced sample at step i-3.

calculation by Teo and Lee[10] were employed in the fitting procedure. The agreement of the calculated and observed curve is indicated by the $R$-index defined by

$$R = \sqrt{\frac{\sum(k_i^3\chi_{obsd}(k_i) - k_i^3\chi_{calcd}(k_i))^2}{\sum(k_i^3\chi_{obsd}(k_i))^2}} \quad (2)$$

where the summation is over all the data points. Fourier transformation of (1) multiplied by $k^3$ gives the so-called radial structure function.[11]

## Results

**Observed Spectra for Alkoxide Method.** The EXAFS spectra of the material at the first three stages of the alkoxide method in Table Ia are almost the same, and the one for the dried sample is shown in Figure 1a. A simple oscillation is visible, and lowering the temperature to 77 K has little effect on the spectra. These indicate that the material does not have an ordered structure beyond the nearest shell at these earlier stages of the preparation.

After the calcination the materials show more complicated spectra due to the contributions from several shells, reflecting that the structure around Co atoms becomes more ordered. In addition, the spectra vary with the calcination temperature. As representative ones, EXAFS spectra obtained by the samples calcined at 723 K for 4 h and at 973 K for 4 h are shown in Figure 1b,c. It is apparent that these two represent different neighborhoods around the Co atoms.

The final step of the catalyst preparation is the reduction. The reduced sample shows similar EXAFS spectra regardless of the calcination temperature, depending only on the reducing conditions. A typical spectrum is shown in Figure 1d for the sample calcined at 723 K for 4 h and reduced at 973 K for 4 h. The interpretation of the EXAFS spectra described here is not so simple and will be thoroughly discussed in the later section.

(8) Sayers, D.; Stern, E. A.; Lytle, F. W. *Phys. Rev. Lett.* **1971**, *27*, 1204–1207.
(9) Stern, E. A. *Phys. Rev. B* **1974**, *B10*, 3027–3037.
(10) Teo, B. K.; Lee, P. A. *J. Am. Chem. Soc.* **1979**, *101*, 2815–2832.
(11) Sinfelt, J. H.; Via, G. H.; Lytle, F. W. *J. Chem. Phys.* **1980**, *72*, 4832–4844.

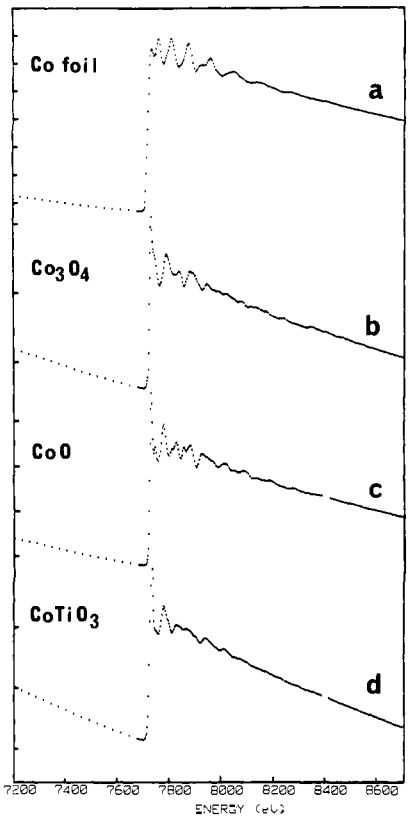


**Figure 3.** EXAFS spectra of reference compounds: (a) Co foil, (b) $Co_3O_4$, (c) CoO, (d) $CoTiO_3$ powder.

**Observed Spectra for Impregnation Method and the Comparison with the Spectra of Reference Compounds.** The EXAFS spectra obtained at each step of the catalyst preparation by the impregnation method are shown in Figure 2a–d and will be discussed briefly in relation to the EXAFS spectra of the reference compounds Co foil, CoO, $Co_3O_4$, and $CoTiO_3$, shown in Figure 3a–d.

The spectrum of the dried sample shown in Figure 2a resembles that in Figure 1a, indicating that the local structure around the Co atom is not ordered except for the nearest-neighbor shell. After the calcination at 723 K for 4 h, the material shows an extensive EXAFS structure. A comparison of Figure 2b with the spectrum of $Co_3O_4$ shown in Figure 3b clearly indicates that these two are the same and that a bulklike $Co_3O_4$ crystal is formed.

On the other hand, Figure 2c, which is the spectrum of the sample calcined at 923 K, is almost identical with Figure 3d, which is the spectrum of $CoTiO_3$. The formation of $CoTiO_3$ was also confirmed by X-ray diffraction studies. Therefore, a solid-state reaction has occurred to give $CoTiO_3$ even at 923 K.

The reduced sample shows almost the same EXAFS spectrum as the sample made by the alkoxide method. Both have a very similar EXAFS structure to that of Figure 3a, which is the spectrum of Co metal. The difference in the near-edge region comes from the existence of unreduced metal, and the sharp peak in Figures 1d and 2d becomes weaker with the increase in reduction temperature and period.

The implication of the EXAFS spectra of the samples prepared by the impregnation method is clear even without a detailed analysis. It can be concluded just by the comparison of the raw spectra that bulklike $Co_3O_4$ crystal is formed when calcined at 723 K and $CoTiO_3$ is formed at 923 K, and the oxides are then reduced to form Co metal. Indeed, analyses by Fourier transform and least-squares curve fitting confirmed the conclusion above. The Fourier transform showed that neither the oxide nor the metal particle is small enough to show surface effect in EXAFS spectra.

## Discussion

The information obtained by the analysis of the EXAFS spectra reflects the local structure around the Co atom and is complementary to that of the bulk structure acquired from the observation

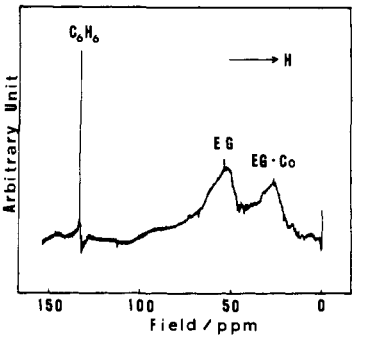


**Figure 4.** C-13 NMR spectrum of the solution of $Co(NO_3)_2$ and ethylene glycol. The coordination of ethylene glycol to Co can be seen.

by electron microscopy. In the following the significance of EXAFS spectra for the understanding of the catalyst preparation procedure by the alkoxide method will be discussed, supported by the results of electron microscopy as well as those of X-ray diffraction, IR, and NMR spectra.

At the first stage of $Co/TiO_2$ catalyst preparation described in Table Ia, cobalt nitrate was dissolved in ethylene glycol at 363 K. The following reaction is expected to take place.

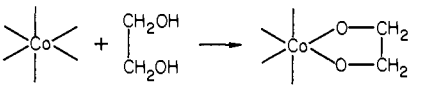


I II III (3)

The formation of cobalt ethylene glycolate is confirmed from the $^{13}C$ NMR spectrum of the solution, which is shown in Figure 4. The major peak at 52 ppm is due to pure ethylene glycol molecule, and a peak shifted toward higher magnetic field should be due to the carbon atoms of $(CH_2O)_2$ which is coordinated to the Co atom.

At the second step titanium isopropoxide is poured into the solution. The reaction must proceed as follows:

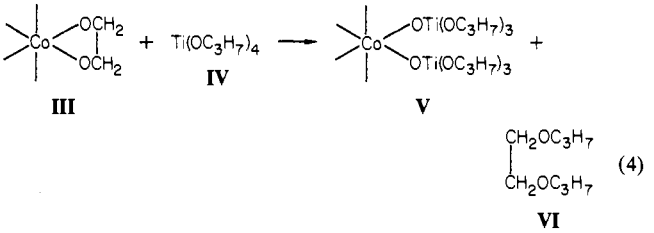


III IV V VI (4)

A hydrolysis of V forms a Co–O–Ti–O network and eventually a gel is formed. Then the gel was dried.

The Fourier transform of the EXAFS of the dried sample is shown in Figure 5a. Only one strong peak is observed at 1.82 Å, and it corresponds to the Co–O distance, since the peak due to Co–O appears at the same position in the reference sample CoO, which is shown in Figure 5b. Small peaks beyond 2 Å in Figure 5a are due to noises, and the second shell, which must be Ti, could not be identified. The IR spectrum also failed to show a band due to the Co–O–Ti bond, which is expected[12] to appear at about 620 $cm^{-1}$. It is, however, certain that reaction 4 has taken place, and the Co–O–Ti bond is formed, because isopropyl alcohol, which is formed by the hydrolysis of VI, is observed by the NMR spectra. In our previous study on $Ni/SiO_2$, the formation of Ni–O–Si bond was confirmed by both EXAFS and IR spectra. Therefore the O–Ti bond is considered to be weaker than O–Si bond and the Co–O–Ti structure does not assume rigid form in this amorphous solid state.

**The Structure of the Calcined Materials.** By calcining the sample at step a-4 of Table I, the environments of Co atom become more ordered, and in addition, structural changes must have occurred during the calcination procedure, because EXAFS os-

(12) Bradley, D. C.; Mehrotra, R. C.; Gaur, D. P. "Metal Alkoxides"; Academic Press: London, 1978; p 118.

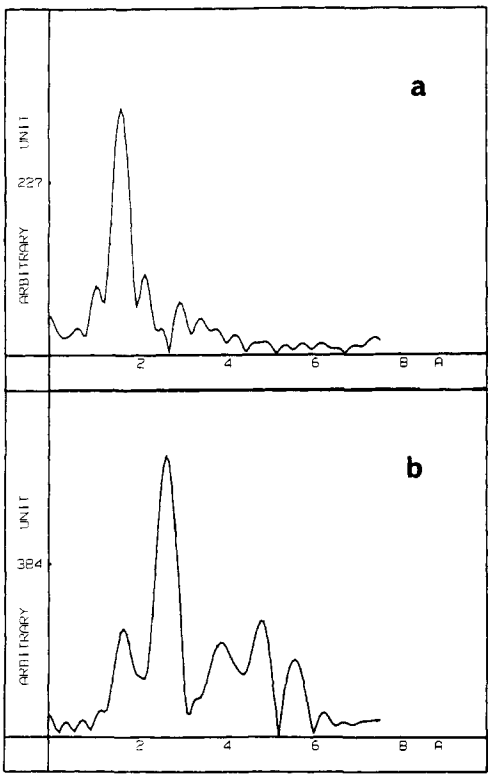


**Figure 5.** Fourier transforms of the EXAFS spectra of (a) the dried sample shown in Figure 1a and (b) CoO shown in Figure 3c.

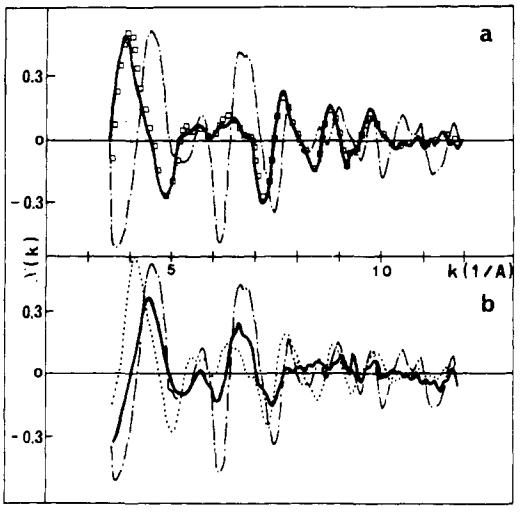


**Figure 6.** (a) Comparison of the extracted oscillation of the EXAFS of the calcined sample at 973 K (bold line) with those of $CoTiO_3$ (square) and $Co_3O_4$ (chain). (b) Comparison of the extracted oscillation of the calcined sample at 723 K (bold line) with those of $CoTiO_3$ (dots) and $Co_3O_4$ (chain).

cillation becomes prominent and also varies with the calcination condition, as already shown in Figure 1b,c. The complicated structures indicate the appearance of several shells.

In the previous experiment on the $Ni/SiO_2$ system NiO microcrystal was formed at this stage. It is too small to be observed by the electron microscope but large enough to show almost the same EXAFS spectra as NiO crystal. The EXAFS spectrum of CoO shown in Figure 3c is, however, markedly different from those shown in Figure 1b,c. Instead, EXAFS spectra of $Co_3O_4$ and $CoTiO_3$ shown in Figure 3b,d bear close resemblance. In order to make a clear identification, a detailed comparison of the extracted oscillation is made in Figure 6. It can easily be concluded from Figure 6a that it is $CoTiO_3$ which is formed in the sample calcined at 973 K. Indeed, the Fourier transforms of both spectra are almost identical, as shown in Figure 7.

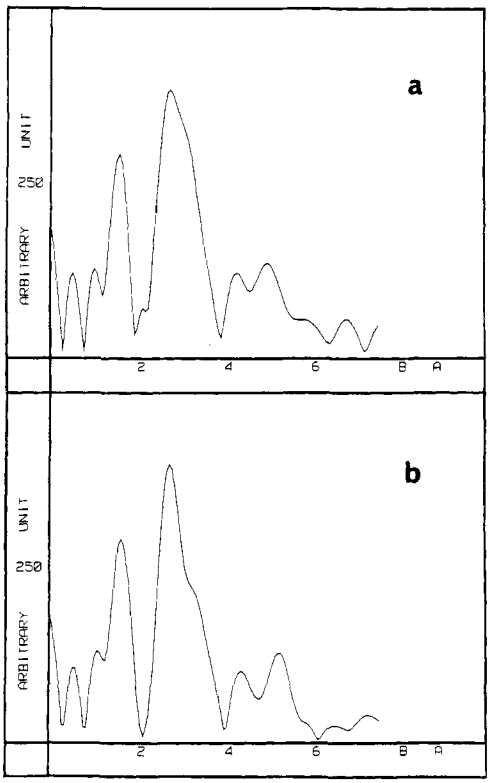


**Figure 7.** Fourier transforms of the EXAFS spectra of (a) the calcined sample at 973 K shown in Figure 1c and (b) the reference sample $CoTiO_3$ shown in Figure 3c.

The oscillation of the sample calcined at 723 K, shown in Figure 6b, is not the same as that of $CoTiO_3$ or $Co_3O_4$, but the spectrum is closer to that of $Co_3O_4$ than those of other reference compounds. Near-edge structure also indicates that Co atoms in this material have a similar environment as $Co_3O_4$. As is seen from Figures 1 and 3, the near-edge structure of those compounds with divalent Co such as CoO and $CoTiO_3$ are sharp, but that of $Co_3O_4$ or this material is somewhat broader.

A radial structure function of this material is shown in Figure 8, together with that of $Co_3O_4$. In order to make a comparison meaningful, the same $k$ range (3.6–12.5 $Å^{-1}$) was used for the calculation of the Fourier transformation. Although the overall structure looks different (that is, peak heights of Figure 8a decrease with increasing distances), the position of every peak coincides exactly. $Co_3O_4$, being a normal spinel, has 16 $Co^{3+}$ atoms (Co($O_h$)) surrounded by six oxygen atoms at 2.02 Å and eight $Co^{2+}$ atoms (Co($T_d$)) surrounded by four oxygen atoms at 1.75 Å in a unit cell. The mean Co–O distance is 1.93 Å, which is appreciably shorter than that of CoO (2.13 Å) and $CoTiO_3$ (2.13 Å). The first peak in Figure 8b corresponds to the two unresolved Co–O distances, and the second one is due to the Co–Co distance at 2.86 Å. Several shells consisting of Co and O contribute to the third and fourth peaks.

The nearest-neighbor distance of the sample calcined at 723 K was determined to be 1.93 Å by the least-squares fit using the parameters[10] for Co–O scattering. The same procedure for $Co_3O_4$ gave 1.90 Å. They agree very well with the reported average Co–O distance of $Co_3O_4$ (1.95 Å). The second peak was identified to be due to Co–Co scattering of $Co_3O_4$ by the curve-fitting method. Figure 9 shows the comparison of the inverse Fourier transform of the second peak with the best-fit curve employing parameters for Co–Co scattering and assuming the Co–Co distance of 2.80 Å. It is almost the same as that obtained by the analysis of the EXAFS of $Co_3O_4$ (2.83 Å) and reported value (2.86 Å) based on X-ray diffraction studies. Therefore the EXAFS spectra suggest that it is $Co_3O_4$ which is formed in the material calcined at 723 K. The difference between parts a and b of Figure 8 can be rationalized if one takes the surface effect into account; the cluster is so small that the number of atoms at distant shell

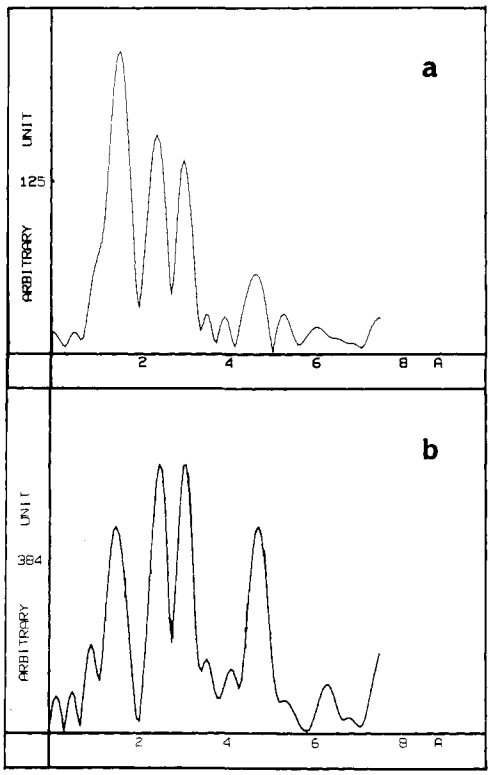


**Figure 8.** Radial structure function of the sample calcined at 723 K (a) and of $Co_3O_4$ powder (b). Notice that the peak positions are the same. Transform range: 3.6–12.5 $Å^{-1}$.

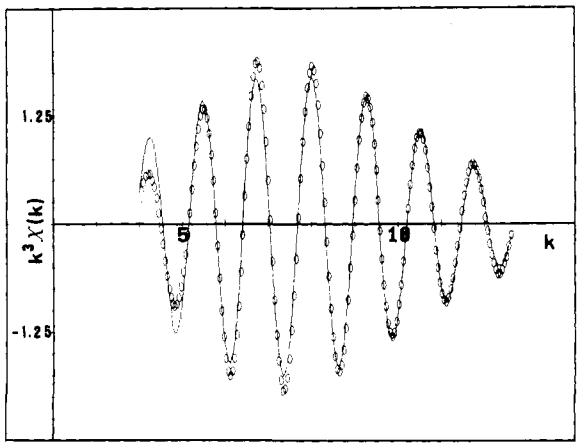


**Figure 9.** Comparison of the inverse Fourier transform of the second peak of Figure 8a with the best-fit curve assuming Co–Co scattering. The parameters used are listed in Table II.

decreases rapidly with distance.

Particle size effects on the EXAFS spectrum have previously been discussed by Greegor and Lytle[13] for metal clusters. They have proposed a figure by which particle sizes can be estimated from the relative intensities of the shells by assuming sphere, cube, or disk shape. The method is, however, not applicable to the present system since the crystal structure is much more complicated. In order to estimate the particle size we have assumed that the particle is cubic and that the spinel structure is retained in this small $Co_3O_4$ cluster. As described above, the spinel structure has two different kinds of Co atoms. Therefore the calculations of the coordination number are performed for each kind, sequentially expanding the cluster size as is shown in Figure 10a. The calculated ratio of $\bar{N}_j/N_j$ as a function of the particle size is shown in Figure 10b, where $\bar{N}_j$ is the average coordination number of the cluster and $N_j$ is the coordination number of the

(13) Greegor, R. B.; Lytle, F. W. *J. Catal.* **1980**, *63*, 476–486.

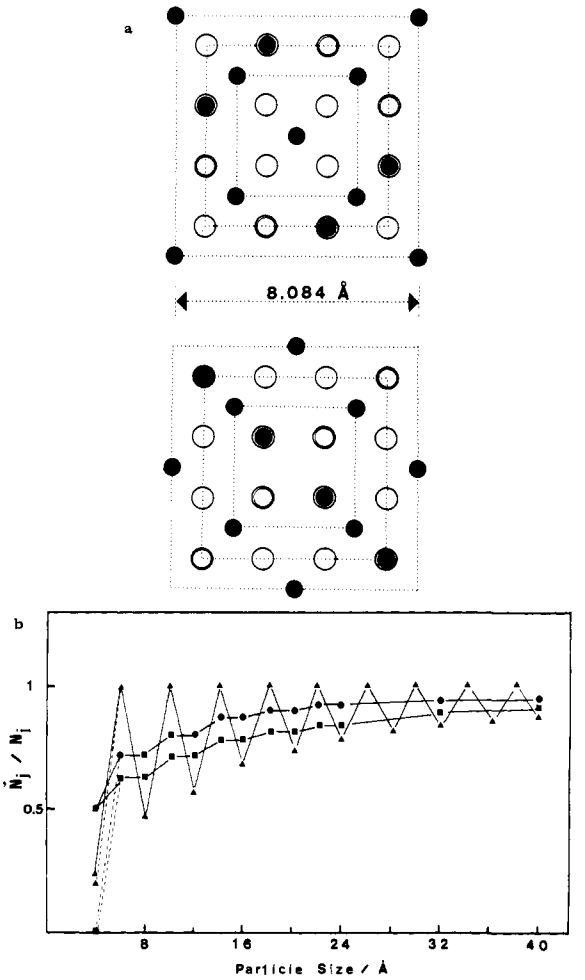


**Figure 10.** (a) Crystal structure of $Co_3O_4$ and the cluster sizes used for the calculation of the average coordination number $\bar{N}_j$. (b) Ratio of $\bar{N}_j/N_j$ calculated by sequentially expanding the cluster size as is shown in (a). ▲ represents the results for Co(Td)–O (1.75 Å), ● for Co(Oh)–O (2.02 Å), and ■ for Co–Co (2.80 Å), respectively.

$j$th sphere of an infinite crystal. The results of the calculation for the first few coordination spheres are shown. The oscillation of $\bar{N}_j/N_j$ is due to the termination effect.

The value of $\bar{N}_j/N_j$ determined by the comparison of the calcined sample with the reference sample $Co_3O_4$ is 0.5 for the first peak, whcih corresponds to the average of the two kinds of Co–O. By the use of this value and Figure 10b, the average particle size of the calcined sample is estimated to be 6–8 Å, which is comparable to the size of the unit cell ($a = b = c = 8.086$ Å). Of course the figure should not be considered accurate, because the clusters are not necessarily cubic, and there must be a wide distribution in size. Nevertheless, it will serve as a rough estimate of the cluster size. There may be a propensity for the kind of atoms that are exposed. Such preference also has an effect on the relative intensities, but it will not alter the above estimate very much.

On the other hand, the Fourier transform of the EXAFS for the material prepared by the impregnation method and calcined at 723 K is almost the same as that of $Co_3O_4$ powder, as described before, indicating that the particle size is large enough in the EXAFS scale.

In Table II are summarized the best-fit values of some structural parameters of the reference compounds and of the materials calcined under different conditions, together with the interatomic distances determined by X-ray diffraction measurements. The values obtained by EXAFS for the reference compounds show excellent agreement with those by X-ray diffraction studies.

Before starting this series of research, we had anticipated that metal–O–Ti (or Si) bonds formed in the gel must be maintained after the calcination because of the modest temperature applied (723–973 K). In the previous report on $Ni/SiO_2$, however, the

Table II. Best-Fit Values of Some of the Structural Parameters of the Samples and of the Reference Materials Determined from EXAFS Data and Interatomic Distances Obtained by X-ray Diffraction Studies for the Reference Materials

| material | neighbor atom | | no. | distance, Å: from X-ray[a] | distance, Å: from EXAFS | $\sigma^2$, Å$^2$ | $R$ |
|---|---|---|---|---|---|---|---|
| CoO | 1st | O | 6 | 2.134 | 2.10 | *b* | 0.023 |
| | 2nd | Co | 12 | 3.018 | 3.00 | 0.005 | 0.012 |
| $Co_3O_4$ | 1st | O | 4 | 1.750 | 1.90 | *b* | 0.23 |
| | 2nd | O | 6 | 2.021 | | | |
| | 3rd | Co | 6 | 2.858 | 2.83 | 0.006 | 0.010 |
| $CoTiO_3$ | 1st | O | 2 | 2.042 | 2.06 | 0.002 | 0.066 |
| | 2nd | O | 4 | 2.167 | | | |
| $Co/TiO_2$ cal. 723 K | 1st | O | | | 1.93 | 0.001 | 0.15 |
| | 2nd | Co | | | 2.80 | 0.003 | 0.027 |
| $Co/TiO_2$ cal. 973 K | 1st | O | | | 2.04 | 0.002 | 0.066 |

[a] Calculated from the data shown in: Wyckoff, R. W. G. "Crystal Structures"; Interscience: New York, 1948; Vol. 2. [b] Least-squares fitting gave negative values as the best fit.

formation of tiny NiO clusters by the calcination was observed. In this study it was also found that Co atoms exist as oxides. The nature of oxide, however, varies depending upon the temperature of the heat treatment. The original purpose of this study was to confirm whether or not the conclusion obtained from $Ni/SiO_2$ preparation procedure is applicable to other systems. We find that the same conclusion can be drawn in this $Co/TiO_2$ catalyst preparation; small oxide clusters are uniformly distributed among the support in the alkoxide method, while oxide particles are large in the impregnation method, and it is the size of the oxide cluster which makes the difference in the resultant catalyst.

Another important result obtained here is that the major structural change has occurred during the calcination process and that the resultant species differ depending on the calcination temperature, in addition to the difference due to the preparation method. Although numerous investigations[14-16] have been carried out on the nature of the calcination process of oxidic (calcined) $Co/Al_2O_3$ catalyst prepared by the impregnation method, there seems to be no report concerning the structure of $Co/TiO_2$ catalysts. In the following our findings are compared with those previously obtained for the $Co/Al_2O_3$ system.

Chin and Hercules[14] observed that the ESCA peak of Co on $Al_2O_3$ shifts from 781.6 to 780.6 eV when the concentration of Co is varied from 2 to 30%. Also when the temperature is raised, the peak shifts toward high energy at high concentration. They attributed the higher energy peak to $CoAl_2O_4$ and the lower one to $Co_3O_4$ and gave the following interpretation. At low calcination temperature $CoAl_2O_4$ is formed because of the diffusion of Co ions into the tetrahedral or octahedral sites of $\gamma$-$Al_2O_3$, which is a defect spinel. As the metal loading is increased, the segregation of $Co_3O_4$ occurs, the ESCA spectrum approaching that of oxide. At high temperature (873 K) a greater proportion of Co ions diffuses into the alumina lattice, making $CoAl_2O_4$ the major surface species. Later Greegor et al.[16] confirmed the structural difference with concentration by observing the change in coordination number in EXAFS and in the X-ray absorption edge structure. The reaction of a metal with $\gamma$-$Al_2O_3$ support has also been reported by Friedman et al.[17] They observed the formation of $CuAl_2O_4$ at high calcination temperature (1173 K) while CuO is formed at low temperature (773 K).

Our observations about the calcined $Co/TiO_2$ catalyst are almost in parallel with those described above. Each of the Fourier transforms of the materials studied here has well-marked characteristics, providing convincing evidence that the resultant species

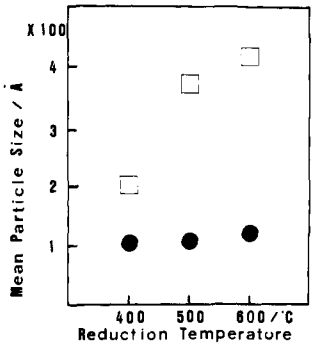


Figure 11. Dependence of the particle size distribution on the reduction temperature determined by electron microscopy for the catalyst prepared by the alkoxide method through different calcination temperature: (□) sample calcined at 723 K and the precedent oxide is $Co_3O_4$; (●) sample calcined at 973 K and the precedent oxide is $CoTiO_3$.

varies with the calcination temperature. Therefore it will be a general phenomenon that bulklike oxide, probably in the largest oxidation number possible, is formed at low calcination temperature and that the metal–support interaction increases with the temperature, forming complex oxide with the support.

**Structure of the Reduced Catalyst.** The final step of the supported metal catalyst preparation is the reduction. EXAFS spectra of fully reduced samples are independent of the calcination temperature and show no particle size effect; relative intensities of the peaks of the radial structure function are almost the same. This indicates that the size of the metal particles is too large to show size effect in EXAFS (>20 Å[13]) under the metal loading studied, although the precedent oxide is sometimes very small (<10 Å) as previously discussed.

On the other hand, an electron microscopic study showed that the species of the oxide strongly affects the metal size of the reduced catalyst. The metal particle sizes of the catalyst prepared by reducing the sample calcined at 723 or 973 K at several reducing temperatures are shown in Figure 11. The particle sizes are rather large, because the measurements were made on the sample with high Co concentration (10%) on which EXAFS were obtained. The material calcined at 973 K gives almost the same metal size regardless of the range of the reduction temperature employed. That is, the metal particle does not grow. On the other hand, the size of the metal particle prepared from the material calcined at 723 K depends strongly on the reducing temperature. The higher the temperature is, the larger is the size of the metal particles formed. The samples prepared by the impregnation method showed a similar but less prominent tendency, because the particles are much larger and have wider distribution in size.

At this stage the reason for this different behavior is not apparent. As was already seen, the difference in the calcination condition results in small $Co_3O_4$ clusters at low temperature and in $CoTiO_3$ at high temperature, and also the cluster size of $Co_3O_4$ is so small that the surface effect is evident from the EXAFS spectra. A growth of the metal particle is considered to occur by the diffusion on the surface of the support. Therefore there must be some reason in the sample calcined at 973 K to prevent Co atoms from moving around.

$TiO_2$ has two polymorphic forms, anatase and rutile. The former is stable at low temperature, and the latter is stable above about 900 K.[18] Therefore the structure of the support is different for the materials calcined at 723 and 973 K, and it may be the diffusion coefficient that makes the difference. A more conceivable reason is, however, that $CoTiO_3$ crystallites formed at high calcination temperature are not isolated from the support but bound by chemical bond to the surface of the support, and consequently hard to move. Independent of the true reason, it is important that the metal particle size does not grow during the reduction in order to make small metal particles of homogeneous size on a support. On the other hand, tiny $Co_3O_4$ clusters formed at low calcination

(14) Chin, R. L.; Hercules, D. M. *J. Phys. Chem.* **1982**, *86*, 360–367.
(15) Pope, D.; Walker, D. S.; Mossi, R. L. *J. Catal.* **1977**, *47*, 33–47.
(16) Greegor, R. B.; Lytle, F. W.; Chin, R. L.; Hercules, D. M. *J. Phys. Chem.* **1981**, *85*, 1232–1235.
(17) Friedman, R. M.; Freeman, J. J.; Lytle, F. R. *J. Catal.* **1978**, *55*, 10–28.
(18) Rao, C. N. R. *Can. J. Chem.* **1961**, *39*, 498–500.

temperature do not have any chemical bond with $TiO_2$ support and can easily move around, aided by their small sizes. As a result, the size grows with reduction temperature.

## Conclusion

It is clear from the analysis of EXAFS that different oxides with various sizes are formed depending on the preparation method and on the calcination temperature. The structure of $TiO_2$ supported Co catalyst, which is prepared by reducing the oxides, strongly depends on the type and size of the oxides. Very small clusters of oxides are formed in the preparation by the alkoxide method at the calcination stage, which makes the size of metal particles of the reduced catalyst small and homogeneous. These conclusions are in very good accordance with those obtained previously for the $Ni/SiO_2$ catalyst.

**Registry No.** Co, 7440-48-4; $TiO_2$, 13463-67-7; $Co_3O_4$, 1308-06-1; $CoTiO_3$, 12017-01-5.

# Carbene Complexes of Zirconium. Synthesis, Structure, and Reactivity with Carbon Monoxide To Afford Coordinated Ketene

**Paul T. Barger, Bernard D. Santarsiero, Justine Armantrout, and John E. Bercaw***

*Contribution No. 6835 from the Arthur Amos Noyes Laboratory of Chemical Physics, California Institute of Technology, Pasadena, California 91125.* *Received July 5, 1983*

**Abstract:** Treatment of $Cp_2Zr(L)(CO)$ ($Cp = C_5H_5$; L = $PMe_3$, CO) with $Cp^*_2ZrH_2$ ($Cp^* = C_5Me_5$) affords zirconium oxycarbene complexes, $Cp_2(L)Zr{=}CHO{-}Zr(X)Cp^*_2$ (L = $PMe_3$, X = H, I; L = CO, X = H), that represent some of the first examples of group 4 metal-to-carbon multiple bonding. The first X-ray diffraction structure determination of a zirconium carbene complex, that of $Cp(PMe_3)Zr{=}CHO{-}Zr(I)Cp^*_2{\cdot}C_6H_6$, is reported ($C2/c$, $a$ = 27.318 (4) Å, $b$ = 19.895 (3) Å, $c$ = 19.932 (5) Å $\beta$ = 132.188 (10)°, $Z$ = 8) and shows a very short Zr–C bond length of 2.117 (7) Å. Treatment of $Cp_2(CO)Zr{=}CHO{-}Zr(H)Cp^*_2$ with $CH_3I$ or $Cp_2(PMe_3)Zr{=}CHO{-}Zr(I)Cp^*_2$ with CO affords the zirconium substituted enediolate zirconacycle, $Cp^*_2ZrOCH{=}C(Zr(I)Cp_2)O$, which has been characterized by an X-ray diffraction study ($P2_1/c$, $a$ = 15.866 (4) Å, $b$ = 10.673 (3) Å, $c$ = 20.561 (4) Å, $\beta$ = 105.5 (2)°, $Z$ = 4). It is proposed that this complex forms by coupling of the zirconoxycarbene and a carbonyl to give a metal-coordinated ketene intermediate that subsequently rearranges to the isolated product. An isotopic crossover experiment has demonstrated that the new carbon–carbon bond is formed in an intramolecular coupling step. The ketene intermediate can be trapped by dissolving $Cp_2(CO)Zr{=}CHO{-}Zr(H)Cp^*_2$ in pyridine, giving $Cp_2(py)Zr(O{=}C{=}CHOZr(H)Cp^*_2)$. Treatment of the isolated ketene complex with $CH_3I$ in benzene gives the enediolate zirconocycle; in pyridine $Cp_2(py)Zr(O{=}C{=}CHOZr(I)Cp^*_2)$ can be observed spectroscopically.

Bis(pentamethylcyclopentadienyl)zirconium hydrides have proven to be useful reagents for the reduction of transition-metal-bound carbon monoxide.[1-3] Previous work has demonstrated that these hydrides, in particular $Cp^*_2ZrH_2$ ($Cp^* = \eta^5$-$C_5Me_5$), can add across the carbon–oxygen bond of a carbonyl on a variety of metals to afford a zirconoxycarbene product (eq 1) or may lead to reductive elimination of $H_2$ and rearrangement

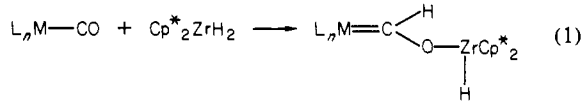

$$L_nM{-}CO + Cp^*_2ZrH_2 \longrightarrow L_nM{=}C(H)O{-}ZrCp^*_2(H) \quad (1)$$

to afford carbonyl-bridged "early" and "late" mixed-metal dimers.[4,5] By the former reaction pathway oxycarbene complexes of niobium,[2] chromium,[3] molybdenum,[3] tungsten,[3] cobalt,[5] and rhodium[5] have been prepared. $Cp^*_2ZrH_2$ also appears to add readily to iron and ruthenium carbonyls,[5] but the carbenes prepared have proven unstable toward further rearrangement.

The first indication that $Cp^*_2ZrH_2$ could reduce carbon monoxide bound to zirconium was the preparation of *cis*-$(Cp^*_2ZrH)_2(\mu$-$OCH{=}CHO{-})$ by the treatment of $Cp^*_2Zr(CO)_2$ with $Cp^*_2ZrH_2$ under an $H_2$ atmosphere,[1,3]

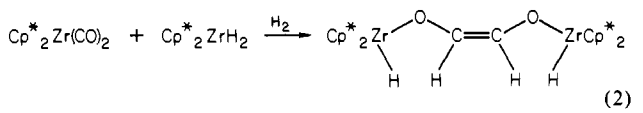

$$Cp^*_2Zr(CO)_2 + Cp^*_2ZrH_2 \xrightarrow{H_2} Cp^*_2Zr(H)O{-}C{=}C(H)O{-}ZrCp^*_2(H) \quad (2)$$

the proposed mechanism[1d] of which is shown in Scheme I. Some aspects of this mechanism have now been tested by preparing models for the proposed intermediates and examining their reactivity.

The initial step of Scheme I is the formation of a zirconoxycarbene of complex of zirconium, similar to those isolated for group 5 and 6 transition metals. Without $H_2$, $Cp^*_2Zr(CO)_2$ and $Cp^*_2ZrH_2$ give a myriad of products, involving a number of transient species. The instability of the intermediate(s) is presumably due to two factors: (1) unfavorable steric interactions of the bulky decamethylzirconocene fragments forced into close contact by the small, two-atom zirconoxycarbene bridge and (2) the presence of an adjacent carbonyl ligand, which may allow for facile decomposition pathways. In our efforts to prepare stable zirconium zirconoxycarbene complexes, these factors have been taken into account.

The only previous reports of carbene complexes of zirconium have been by Schwartz and co-workers. In 1980 the spectroscopic observation of $Cp_2Zr(CH_2)(PPh_2Me)$ was reported, although

$$Cp_2Zr(PPh_2Me)_2 + CH_2{=}PPh_3 \rightarrow Cp_2Zr(CH_2)(PPh_2Me) + PPh_3 + PPh_2Me \quad (3)$$

isolation of the product was prevented by its instability at room temperature under the reaction conditions.[6] More recently, Schwartz has reported the isolation of $Cp_2(L)Zr{=}C(H)(CH_2R)$ (L = $PPh_3$, $PMe_2Ph$; R = *t*-Bu, $C_6H_{11}$, CH(Me)(Et)) as impure oils.[7]

(1) (a) Manriquez, J. M.; McAlister, D. R.; Sanner, R. D.; Bercaw, J. E. *J. Am. Chem. Soc.* **1976**, *98*, 6733. (b) Manriquez, J. M.; McAlister, D. R.; Sanner, R. D.; Bercaw, J. E. *Ibid.* **1978**, *100*, 2716. (c) Bercaw, J. E. *Adv. Chem. Ser.* **1978**, *No. 167*, 136. (d) Wolczanski, P. T.; Bercaw, J. E. *Acc. Chem. Res.* **1980**, *13*, 121.
(2) Threlkel, R. S.; Bercaw, J. E. *J. Am. Chem. Soc.* **1981**, *103*, 2650.
(3) Wolczanski, P. T.; Threlkel, R. S.; Bercaw, J. E. *J. Am. Chem. Soc.* **1979**, *101*, 218.
(4) Barger, P. T.; Bercaw, J. E. *J. Organomet. Chem.* **1980**, *201*, C39.
(5) Barger, P. T.; Bercaw, J. E. *Organometallics*, **1984**, *3*, 278-284.

0002-7863/84/1506-5178$01.50/0 